Remote Sensing of Environment 225 (2019) 469–482

Contents lists available at ScienceDirect

Remote Sensing of Environment

journal homepage: www.elsevier.com/locate/rse

CCI soil moisture assessment with SMOS soil moisture and *in situ* data under different environmental conditions and spatial scales in Spain

Á. González-Zamora*, N. Sánchez, M. Pablos, J. Martínez-Fernández

CIALE, Instituto Hispanoluso de Investigaciones Agrarias, University of Salamanca, Duero 12, 37185, Villamayor, Spain

ARTICLE INFO

Keywords:
CCI
SMOS
Soil moisture
Validation

ABSTRACT

In this research, the active, passive and combined Climate Change Initiative (CCI) Soil Moisture (SM) products were evaluated in comparison with *in situ* SM measurements from five networks in Spain that have different spatial and temporal scales, densities and environmental conditions. Three of these networks, namely Rinconada, Morille and the Soil Moisture Measurement Stations Network of the University of Salamanca (REMEDHUS), are small- to medium-scale networks and have high station densities, whereas the other two (Inforiego and FluxNet) are sparse and large-scale networks.

The results of the comparisons with the former v02.2 version (before the inclusion of the SM retrieved by the Soil Moisture and Ocean Salinity mission, SMOS, in the CCI dataset) showed that the combined CCI performed better than the active or passive, affording correlation coefficients (R) above 0.8 and errors between 0.03 and 0.08 $m^3 m^{-3}$ for the area-average, with biases close to zero. Regarding the land uses and environmental conditions, the stations that were located in the agricultural areas and some forested areas showed the best results, and those that were located in pasture and certain specific agricultural locations showed the poorest results.

To test the opportunity of including SMOS in CCI, both datasets were compared over the same areas and coincident periods. After the results, the combined CCI and SMOS SM products matched very well ($R = 0.83$ on average), although the SMOS and CCI under- and overestimate the ground soil moisture measurements, respectively.

Finally, the new version of the combined CCI (v03.2, after including SMOS) showed similar correlations to the previous one, but it significantly reduced the bias, leading to slightly lower errors (RMSD and cRMSD). Hence, it was shown that including SMOS in the CCI database enhanced its performance.

The results in this work may improve knowledge of the CCI SM and its potential applications.

1. Introduction

Nowadays, the importance of the soil moisture (SM) is undeniable. The increasing number of permanent *in situ* SM networks available for potential validation activities (Crow et al., 2012) as well as the recent space missions specifically devoted to globally estimate SM (Ochsner et al., 2013) prove the utility of this variable in several fields, such as the Agriculture, Climatology, Meteorology or Hydrology.

Since the late 1970s, a great variety of microwave sensors has been used to measure SM (Petropoulos et al., 2015; Mohanty et al., 2017). Microwave spectrum is the most suitable for estimating SM because this bandwidth is sensitive to the dielectric properties of land surfaces, particularly to increases in the soil dielectric constant when the fraction of soil water content increases. The remote sensing of SM is based on the measurement of the emitted or reflected electromagnetic energy coming from the Earth surface, using a passive (radiometer) or an active (radar) sensor, respectively. The former measures the brightness temperature and the last the radar backscatter coefficient (Singh et al., 2015).

Recent missions dedicated to SM monitoring rely on the use of L-band (1–2 GHz) radiometers. This band has a larger soil-penetration depth than higher microwave frequencies, omitting the presence of vegetation “up to moderate densities” (Jackson and Schmugge, 1991). In November 2009, the European Space Agency (ESA) launched the first satellite designed to observe the global SM, the Soil Moisture and Ocean Salinity (SMOS), which has since been successfully providing SM data, using an L-band interferometric radiometer (Kerr et al., 2010). In January 2015, the National Aeronautics and Space Administration (NASA) launched the Soil Moisture Active Passive (SMAP) mission, which was specifically dedicated to measure SM and the freeze/thaw state. It currently uses an L-band real aperture radiometer (Entekhabi et al., 2010) because, unfortunately, the synthetic aperture radar

* Corresponding author at: Instituto Hispanoluso de Investigaciones Agrarias, University of Salamanca, Duero 12, 37185, Villamayor, Spain.
E-mail addresses: aglezzamora@usal.es (Á. González-Zamora), nilda@usal.es (N. Sánchez), mpablos@usal.es (M. Pablos), jmf@usal.es (J. Martínez-Fernández).

https://doi.org/10.1016/j.rse.2018.02.010
Received 31 March 2017; Received in revised form 20 December 2017; Accepted 8 February 2018
Available online 13 February 2018
0034-4257/ © 2018 Elsevier Inc. All rights reserved.

stopped working on July 2015. Together with NASA, the Argentina's space agency launched the Aquarius/SAC-D satellite in 2011 (Lagerloef et al., 2008). On board this satellite was an L-band radiometer to acquire the sea surface salinity and a scatterometer for correcting the sea surface roughness, although the radiometer observations over land had also been used to estimate SM (Bindlish et al., 2015).

The Climate Change Initiative (CCI) project realized the potential of integrating all active and passive microwave (L-, C-, X- and Ku-band) satellite sensors to produce a global, consistent and long-term SM database. In this database, three different CCI products exist: one with only active, another with only passive, and a third combined product that blends both passive and active observations. In the v02.2, sensors operating at C-, X- and Ku-bands have been included, but any L-band sensor (SMOS, Aquarius and SMAP) have not been yet integrated (Dorigo et al., 2015). By contrast, the v03.2 includes the L-band SMOS observations (Dorigo et al., 2017). The v02.2 and previous versions have been evaluated and validated worldwide (Dorigo et al., 2015; An et al., 2016; McNally et al., 2016) and used for different applications, particularly the combined CCI SM product for crop monitoring (Sakai et al., 2016) and agricultural drought assessment (Carrão et al., 2016; Rahmani et al., 2016).

The new version v03.2 includes, in addition to the SMOS observations, improvements in the algorithm to reduce errors associated with the product. This new version showed an important increase of the spatio-temporal coverage and it is expected to improve the results showed by previous versions (Dorigo et al., 2017).

The main lines being investigated in this work were, in the first place, to assess the v02.2 CCI over Spain using *in situ* SM measurements from five networks with different spatial and temporal scales, densities and environmental conditions. Three of these networks, namely the Soil Moisture Measurement Stations Network of the University of Salamanca (REMEDHUS), Morille and Rinconada, are small- to medium-scale, high-density networks, whereas the other two (Inforiego and FluxNet) are sparse and large-scale networks. These networks provided data from 1999 to the present during different periods, thus enabling us to compare a considerable amount of data to the CCI datasets at different scales and under different environmental conditions. Since the CCI SM is a long-term dataset, its seasonality and anomalies were also assessed.

Secondly, with the aim or testing the feasibility of including SMOS in a new version, the passive and combined CCI SM v02.2 and SMOS L2 SM products were compared over the same areas and coincident period for both datasets. These comparisons were done against *in situ* measurements, as well as with each dataset against each other they were inter-compared between them.

Finally, the new CCI SM v03.2 was also tested over the same areas and periods to study the impact of including SMOS in this new database and quantify the expected improvement over the previous version (v02.2).

2. Datasets and methodology

2.1. Remotely sensed products

2.1.1. CCI SM products

The passive and combined CCI SM products starts in 1978 and the active product starts in 1991. All the three products span to 2014 for the v02.2 and to 2015 in the v03.2, with a spatial resolution of 0.25° and a daily temporal resolution.

In v02.2, the active CCI SM product is based on backscatter measurements from the Active Microwave Instrument (AMI) wind scatterometer onboard European Remote Sensing Satellites (ERS) 1 and 2 (Wagner et al., 1999) and the Advanced SCATterometer (ASCAT) onboard the Meteorological Operational Satellite (MetOp-A) (Wagner et al., 2013). However, for the v03.2, the backscatter measurements from MetOp-B ASCAT are integrated (Wagner et al., 2013). All those sensor designs are similar and operate in the C-band (5.3 GHz). In both versions, the active SM estimates are computed using the WARP 5.5 change detection method (Naeimi et al., 2009) and the ascending and descending orbits are scaled to the more recent scatterometer time series by applying a cumulative distribution function (CDF) matching (Liu et al., 2011; Liu et al., 2012). The SM estimations are provided for the first few centimeters of the soil in percentage of saturation, adjusting the lowest and highest values of the series to 0 and 100%, respectively.

The passive CCI SM v02.2 product merges the remotely sensed brightness temperature from the Scanning Multi-channel Microwave Radiometer (SMMR) onboard the Nimbus 7 satellite (Owe et al., 2008), the Special Sensor Microwave Imagers (SSM/I) from the Defense Meteorological Satellite Program (DMSP) (Jackson, 1997), the Microwave Imager from the Tropical Rainfall Measuring Mission (TRMM) (Gao et al., 2006), the AMSR-E and AMSR2 sensors, respectively (Njoku et al., 2003), and the WindSAT onboard the Coriolis platform (Parinussa et al., 2012). In addition, the v03.2 adds the brightness temperatures from SMOS (Kerr et al., 2010). The brightness temperatures are converted into SM values by applying the dual channel VUA-NASA Land Parameter Retrieval Model (LPRM) version 3 (Owe et al., 2008). The passive sensors operate in different bandwidths: Ku-band (19.3 GHz), X-band (10.7 GHz), C-band (6.6/6.9 GHz) and L-band (1.4 GHz). Only the SM estimates from night-time passes are scaled by applying a CDF matching, using the more recent radiometer time-series as reference (Liu et al., 2011; Liu et al., 2012). The passive SM is provided in $m^3\,m^{-3}$, being representative of a soil layer from the top few millimeters to several centimeters deep depending on the channel and soil wetness (Kuria et al., 2007).

The merged CCI SM product is a combination of the aforementioned active and passive CCI SM products. It homogenizes and merge all the microwave-based observations. In v02.2, the scaling references of the CDF matching correspond to AMSR2 and MetOp-A ASCAT. In addition, the vegetation density is used as a threshold to generate the combined CCI SM, being moderate vegetation the threshold for the passive products and the low vegetation for the active products (Dorigo et al., 2015). In v03.2, the references are SMOS and MetOp-B ASCAT, and, instead of vegetation thresholds, a weighted average was applied for blending the active and passive measurements (Dorigo et al., 2017).

Quality flags were included with all the three different products. In this research, these flags were used to filter the data, and thus pixels with snow cover, temperatures below 273 K, dense vegetation or failed SM retrieval were discarded (Holmes et al., 2009; Dee et al., 2011).

2.1.2. SMOS product

The SMOS L2 SM User Data Product (SMDUP2) v6.20 time series from June 2010 to December 2014 were used. The soil moisture is retrieved with a spatial resolution of around 30–50 km and projected to a 15-km Icosahedral Snyder Equal Area Earth (ISEA-4H9) grid, with an accuracy goal of $0.04\,m^3\,m^{-3}$ (Kerr et al., 2012). Each SMOS pixel is known as Discrete Global Grid (DGG). The data quality index (DQX) and radio-frequency interference (RFI) flags were used to filter the time series, as proposed by González-Zamora et al. (2015). The SMOS L2 SM product is provided in two orbits, *i.e.*, ascending and descending (6:00 am and 6:00 pm local time, respectively), even though only one orbit is available on most days. When possible, a daily average from both orbits was calculated.

2.2. In situ SM networks

Crow et al. (2012) classified soil moisture networks depending on stations density and spatial scale range into two types: sparse, large-scale networks ($> 10{,}000\,km^2$) and dense, small- to medium-scale networks ($< 10{,}000\,km^2$). In this study, SM stations from five different networks around Spain were used, namely REMEDHUS, Inforiego, Morille, Rinconada and FluxNet (Fig. 1 and Tables 1 and 2).

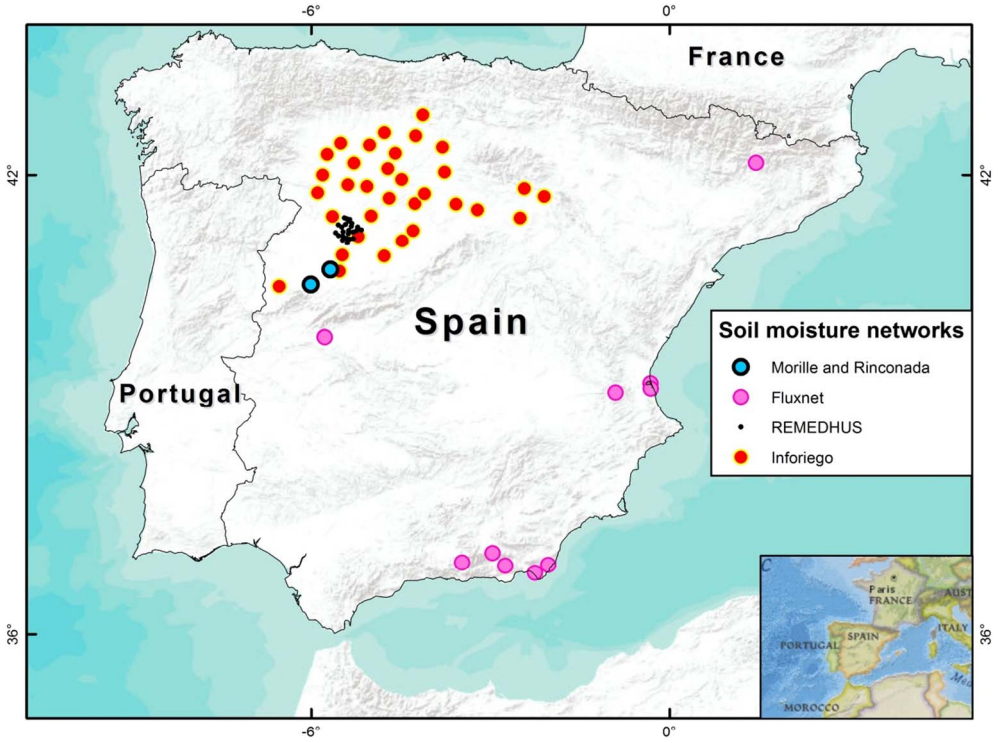

Fig. 1. Locations of the different *in situ* stations used in this research.

REMEDHUS SM data are nested in the International Soil Moisture Network (Dorigo et al., 2011), which has provided continuous data since 1999 to validate remotely sensed SM products (Ceballos et al., 2005; Sánchez et al., 2012; González-Zamora et al., 2016; Piles et al., 2016). REMEDHUS covers an agricultural area (1300 km^2) in the Duero Basin, which has a continental semiarid Mediterranean climate. The main crops are rainfed cereals and, to a lesser extent, irrigated crops and vineyards. Some scattered forest and pasture areas are also present. This network was equipped with 23 Time Domain Reflectometry (TDR) stations from 1999 to 2009 (Martínez-Fernández and Ceballos, 2003), which collect measurements fortnightly, and 24 capacitance probe (Hydra Probes, Stevens Water Monitoring System, Inc.) stations from 2005 to the present day, which collect measurements every hour (Gumuzzio et al., 2016). Both sensor types explore the top 5 cm of the soil. In the case of the Hydra probes, a daily-average of each station was used for the validation.

The Inforiego network covers the main section of the Duero Basin (≈65,000 km^2), which has a continental Mediterranean climate (González-Zamora et al., 2015). The main crops in this agricultural region are rainfed cereals and irrigated summer crops. This SM network upgrades an existing meteorological network that was dedicated to irrigation management (http://www.inforiego.org/). Seventeen stations were operational from July 2012 to July 2013 (Inforiego12) and an additional 16 stations from August 2013 to August 2014 (Inforiego13). In both cases, Hydra probes collected measurements at 5 cm depth. In Gumuzzio et al. (2015), the criteria applied for the selection and representativeness of the station locations were explained in terms of environmental characteristics, such as the soil type and land use in the entire area. These stations measured the SM every hour, but a daily average was determined for each station in our work, as with the REMEDHUS network.

The Rinconada network was deployed in a small experimental catchment (62 ha) in the Sistema Central mountains, which has a sub-humid Mediterranean climate. All the SM stations were located in a dense oak (*Quercus pyrenaica Will.*) forest. This network was equipped with 18 TDR stations from 2000 to 2007, which measured the SM fortnightly at 0–5 cm depth (Hernández-Santana et al., 2009).

The Morille network was deployed in a small experimental catchment (35 ha) in the surroundings of the city of Salamanca, which has a continental Mediterranean climate. All the SM stations were located in an open holm oak (*Quercus rotundifolia Lam.*) forest type, called *dehesa*. This network was equipped with 11 TDR stations from 2001 to 2007, which measured the SM fortnightly at 0–5 cm depth (Hernández-Santana et al., 2008).

Some stations were selected from the FluxNet network (Table 2), which is a worldwide network that provides carbon-dioxide flux measurements and water-vapor exchange rates (Baldocchi et al., 2001). SM is also a core parameter that is measured by each FluxNet station. Twelve FluxNet *in situ* SM datasets were acquired in Spain for different monitoring periods and under different environmental conditions. Further information on FluxNet was provided in Running et al. (1999).

Table 1
Characteristics of the REMEDHUS, Morille, Rinconada and Inforiego *in situ* soil moisture networks.

Network	Number of stations	Sensor type	Sampling	Scale	Density	Period	Land use
REMEDHUS	23	TDR	Fortnightly	1300 km^2	Dense network	1999–2009	Agriculture
REMEDHUS	24	Hydra	Hourly	1300 km^2	Dense network	2005–2015	Agriculture
Morille	11	TDR	Fortnightly	35 ha	Dense network	2001–2007	Open forest
Rinconada	18	TDR	Fortnightly	62 ha	Dense network	2000–2007	Dense forest
Inforiego12	17	Hydra	Hourly	65,000 km^2	Sparse network	2012–2013	Agriculture
Inforiego13	16	Hydra	Hourly	65,000 km^2	Sparse network	2013–2014	Agriculture

Table 2
FluxNet *in situ* stations.

FluxNet station	Location	Latitude (°)	Longitude (°)	Altitude (m)	Period	Land use
ES-Agu	Aguamarga	36.9400	−2.0332	201	2006–2013	Shrub
Es-Amo	Amoladeras	36.8336	−2.2523	60	2007–2012	Shrub
ES-CPa	Cortes de Pallás	39.2242	−0.9031	808	2009–2011	Shrub
ES-ES1	El Saler	39.3460	−0.3188	3	1999–2005	Agriculture
ES-ES2	El Saler	39.2756	−0.3153	0	2004–2010	Agriculture
ES-LgS	Laguna Seca	37.0979	−2.9658	2264	2007–2009	Shrub
ES-LJu	Llano de los Juanes	36.9266	−2.7521	1618	2005–2011	Shrub
ES-LM1	Majadas de Tiétar	39.9427	−5.7787	265	2014	Open forest
ES-LM2	Majadas de Tiétar	39.9427	−5.7787	265	2014	Open forest
ES-LMa	Majadas de Tiétar	39.9415	−5.7734	266	2004–2011	Open forest
ES-Ln1	Lanjarón	36.9721	−3.4739	2304	2008–2009	Shrub
ES-VDA	Vall d'Alinyà	42.1522	1.4485	1771	2004–2008	Pasture

2.3. Methodology

The volumetric measurements of the stations were converted into percentages prior to validating the active CCI product because it was provided in percentages. The time series were normalized between 0 and 100% (corresponding to the lowest and highest SM values of the time series) and, similar to what was used for the CCI active product retrieval. Thus, the active product was compared to the *in situ* time series in percentages, and the passive and combined products were directly compared to *in situ* time series in volumetric units.

The first analysis consists in the appraisal of the CCI SM v02.2, before the inclusion of SMOS. The three products were compared to *in situ* measurements provided by the five SM networks. The time series from the *in situ* measurements were previously collocated with CCI SM time series for their coincident period. The validation was proposed at two scales depending on the network type. First, a comparison at the dense networks (Morille, Rinconada and REMEDHUS, all of which were small- to medium-scale) was performed using the area-averaged SM, both the *in situ* and the CCI SM. Second, the Inforiego and FluxNet stations were compared to the CCI SM products using only the stations within each pixel of each CCI SM product. Although REMEDHUS was considered a dense network, this analysis at the pixel-scale was also conducted to enhance the comparison.

The combined CCI SM v02.2 product was also assessed in terms of seasonality and anomalies over the REMEDHUS area. Both indicators are usually used for long time series with the aim to test the satellite data suitability when long-term data are required (Makridakis et al., 1998; Dente et al., 2013). For this purpose, the methodology described in Makridakis et al. (1998) was used for a period of 13 years (2002–2014), in which the SM is composed by the trend-cycle component (TC), the seasonal component (S), and the anomaly component (A) in the following way:

$$SM = TC + S + A$$

For estimate of TC, a moving average window with a length of 1 year was applied to the time series. The effect of this smoothing is to remove the seasonal and irregular components (Dente et al., 2013). In order to estimate S, multi-year average for each given day corresponding to the different years of the time series was computed.

Few attempts have been made to compare the CCI with other satellite SM products not included in CCI (Peng et al., 2015; Pratola et al., 2015). Since the CCI SM v03.2 includes the SMOS estimations, a further analysis was included to appraise the performance of this inclusion. In addition, several conclusions of the accuracy of both products separately may result from this analysis. Thus, the comparisons of the SMOS L2 and the passive/combined CCI products with the *in situ* SM at the overlapping period (from 2010 to 2014) were analyzed, as was the inter-comparison between the SMOS L2 SM and the different CCI SM v02.2 products. The active CCI product was discarded in this analysis because the SMOS payload is a passive sensor.

Regarding the comparison between CCI and SMOS, an additional analysis was performed to study the intra-pixel (or intra-DGG) spatial variability by applying three interpolation methods to the point-scale measurements in REMEDHUS. The *in situ* measurements (for each study date) were upscaled from the punctual observations to SM maps using three different geostatistical approaches: linear interpolation, natural neighbor and inverse distance weighted (IDW). A detailed description of each method can be found in Burrough (1986). The interpolation was computed at the nominal remote sensing imagery resolutions, *i.e.*, 0.25° for CCI and 15 km for SMOS. The geostatistical procedure integrated the spatial variability instead of a simple station average within a pixel/DGG for the dense networks. This analysis aims to detect if the spatial distribution of stations within a pixel/DGG influenced the validation results and whether the results performed better than those from the arithmetical mean.

Finally, taking advantage of the launch of the v03.2 (February 2017), the combined CCI SM v03.2 product was also compared to *in situ* measurements at the five networks. The validation was performed using the average of the stations within each pixel into the combined CCI SM product, and the area-averaged SM, both the *in situ* and the CCI SM. This additional analysis aims to compare the performance of both CCI versions, thus if the integration of L-band data have improved the new passive CCI SM v03.2 and, by extension, the combined CCI SM v03.2.

In all cases, the results of the comparisons were assessed through the Pearson correlation coefficient (R), bias and errors (root mean square difference, RMSD, and centered RMSD, cRMSD), as performed in most validation experiments of remotely sensed SM (Lacava et al., 2012; McColl et al., 2014; González-Zamora et al., 2015; Piles et al., 2016). These metrics were calculated as follows:

$$R = \frac{\sum_{i=1}^{n}(x_i - \overline{x})(y_i - \overline{y})}{\sqrt{\sum_{i=1}^{n}(x_i - \overline{x})^2}\sqrt{\sum_{i=1}^{n}(y_i - \overline{y})^2}} \quad (1)$$

$$Bias = \frac{\sum_{i=1}^{n}(x_i - y_i)}{n} \quad (2)$$

$$RMSD = \sqrt{\sum_{i=1}^{n}\frac{(x_i - y_i)^2}{n}} \quad (3)$$

$$cRMSD = \sqrt{\frac{\sum_{i=1}^{n}[(x_i - \overline{x}) - (y_i - \overline{y})]^2}{n}} \quad (4)$$

where x_i is the *in situ* observation, y_i is the satellite observation and n is the number of observations. The correlation (Eq. 1) captures the coherence in phase between the estimates and ground observations regardless of existing biases and/or variances. The bias (Eq. 2) is considered the difference between ground and remote observations. Both metrics are independent. The RMSD (Eq. 3) captures the deviation between the ground and remote observations in a quadratic form. However, this metric can be compromised if the bias is large. In this

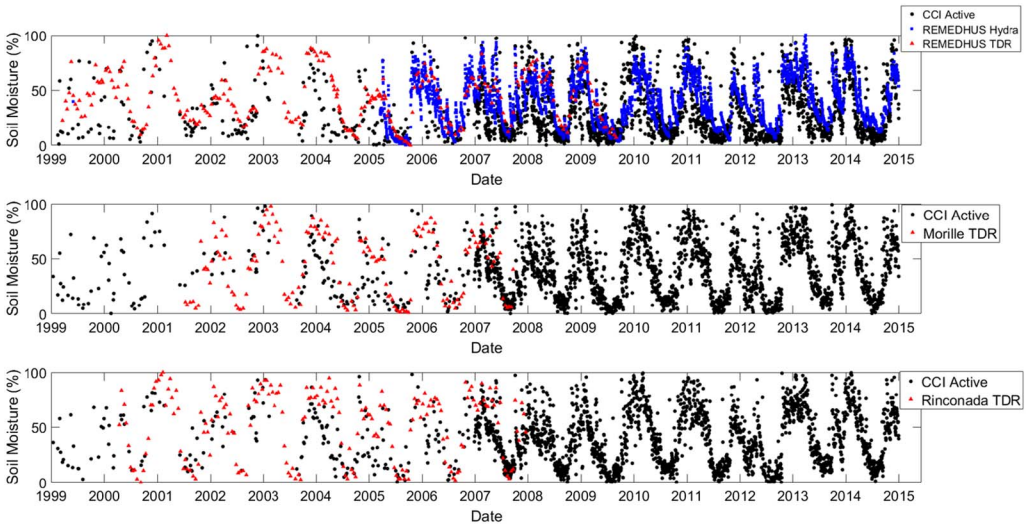

Fig. 2. Soil moisture evolution of the *in situ* SM and active CCI SM v02.2 (area-average) for the REMEDHUS (top), Morille (middle) and Rinconada (bottom) networks.

case it is recommended using cRMSD (Eq. 4), which unbiases the RMSD. Further explanations of these metrics can be found in Entekhabi et al. (2009).

3. Results and discussion

3.1. CCI v02.2 products vs. in situ measurements

3.1.1. Dense networks

The comparison of the three different CCI SM time series v02.2 with the *in situ* SM from the different dense networks (Figs. 2 and 3) revealed that the CCI series had a larger dynamic range than the *in situ*. On the one hand, this effect is more pronounced in the active product due to that it was normalized between the maximum and minimum values of the time series. On the other hand, the combined CCI SM time series showed the best agreement among the different CCI products.

The three CCI dataset followed well the temporal dynamics and the seasonal patterns of the *in situ* datasets, although a certain overestimation was noticeable during the wet periods (winter) and a slightly underestimation during the dry periods (summer). Additionally, the CCI series better matched the higher SM values observed in the Morille and Rinconada networks than those in REMEDHUS. This result is noticeable because Morille and Rinconada correspond to hilly and mountainous forest areas, respectively, whereas REMEDHUS is located over a nearly flat agricultural area.

The low amount of data that were measured in the passive and combined CCI SM time series before mid-2002 was also remarkable (Fig. 3). Until that time, when AMSR-E began operation, the number of sensors that measured soil moisture and the temporal resolution of these data were both very low. The same effect is remarkable in the active CCI SM time series before 2007, when ASCAT began operation (Fig. 2).

The comparisons at the area-average scale of the active and passive CCI SM v02.2 data for the dense networks (Table 3) showed the best correlation and lowest errors for Morille and Rinconada, which could be related to the low-vegetation coverage (only 14% tree cover). Most of the surfaces in this savanna-like landscape are bare soils during several months, mainly during the dry season. Poorer results were found in REMEDHUS (TDR), with lower R and higher errors. However, REMEDHUS (both TDR and Hydra data) showed slightly lower correlations and slightly higher errors than Morille and Rinconada, as suspected from the time series analysis (Figs. 2 and 3). Overall, good results were obtained for the dense networks for both the active and passive products, but the passive better matched the *in situ*

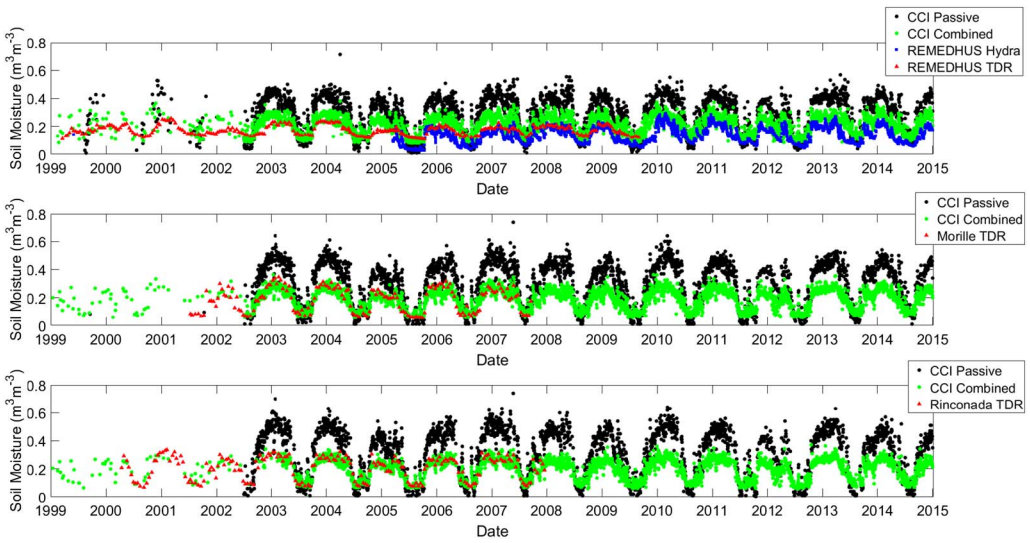

Fig. 3. Soil moisture evolution of the *in situ* SM and passive and combined CCI SM v02.2 (area-average) for the REMEDHUS (top), Morille (middle) and Rinconada (bottom) networks.

Table 3
Results of the comparison between the *in situ* SM with the active (A), passive (P) and combined (C) CCI SM v02.2 (area-average) for Morille, Rinconada and REMEDHUS (TDR and Hydra, separately). All the results are significant at the 0.01 confidence level. The RMSD, cRMSD and bias units for the passive and combined products are $m^3 m^{-3}$, and for the active product are %. (*) Number of coincident data days.

	R			RMSD			cRMSD			Bias			N (days)*		
	A	P	C	A	P	C	A	P	C	A	P	C	A	P	C
Morille	0.91	0.87	0.87	15.1	0.151	0.042	11.3	0.085	0.042	10.0	−0.126	−0.003	12	100	105
Rinconada	0.81	0.93	0.92	19.2	0.151	0.031	17.2	0.086	0.031	8.5	−0.124	0.005	20	87	84
REMEDHUS (TDR)	0.61	0.79	0.75	25.2	0.161	0.057	21.2	0.097	0.045	13.7	−0.128	−0.035	69	156	166
REMEDHUS (Hydra)	0.77	0.82	0.81	17.9	0.179	0.082	16.0	0.087	0.038	8.1	−0.157	−0.072	2337	2694	3273

measurements than the active product. The errors were comparable (~15%), but this result should be cautiously examined because the conversion of the *in situ* stations' units to percentages could have influenced these results. The errors from the passive CCI SM data were higher than those from the other passive products (Gao et al., 2006; Sánchez et al., 2012; Al-Yaari et al., 2014; Chan et al., 2016; Su et al., 2016b), far larger than the typical threshold of 0.04 $m^3 m^{-3}$. A dry bias was obtained in the dense networks in this study for the active product and wet bias for passive product.

The combined CCI SM v02.2 product at the area-average scale showed similar correlations to the passive and higher correlations than the active product (Table 3). However, the errors were reduced from RMSD~0.160 $m^3 m^{-3}$ to RMSD~0.06 $m^3 m^{-3}$ and from cRMSD~0.087 $m^3 m^{-3}$ to RMSD~0.040 $m^3 m^{-3}$ compared to those of the passive product. The bias was close to zero, contrary to findings from recent validation studies performed at other sites with the combined CCI SM (v02.1 and before) product, which showed a general underestimation of the ground SM measurements (Liu et al., 2012; Peng et al., 2015; An et al., 2016). The version in this work (v02.2) apparently performed better. The change in the reference sensors to normalize the passive and active series to AMSR2 and ASCAT, respectively, enabled this version estimates to perform better than those of previous products.

The TDR and Hydra datasets yielded coherent and similar results in terms of the influence of the different types of ground measurements (time interval and number of data) on the validation and, therefore, the amount of data included in the comparison apparently did not influence the results. Accounting for the land uses, we observed surprisingly better performance for the forested areas (Morille and Rinconada) than for the agricultural area of REMEDHUS, where the results were also noteworthy. These results are noticeable because satellite SM validation experiments over forested areas, even if rare, usually show poorer results (Gherboudj et al., 2012) than those in areas with lower vegetation coverage. However, some exceptions exist. Vittucci et al. (2016) compared SMOS SM retrievals in forests and ground measurements to the US SCAN (Soil Climate Analysis) network and gave worse results with respect to low-vegetation areas. Nevertheless, these authors stated that these comparisons can be influenced by the insufficient spatial sampling of ground data. In fact, the correlation coefficients in some of these forest sites were close to or better than 0.7.

In previous research over REMEDHUS (Sánchez et al., 2012; Piles et al., 2014; González-Zamora et al., 2015; Leng et al., 2017), stations located at forest-pasture sites obtained very good correlation results, even though the bias and errors were high. Remotely sensed SM is known to be much more variable in space/time that *in situ* observations (Wagner et al., 1999; González-Zamora et al., 2016). Therefore, the correlation coefficients increased when the correlation analysis was applied to areas with higher water content variability, such as forest-pasture patches. These areas are usually in river valleys and their soils have higher clay content, which can also explain both the higher correlations and higher errors.

The best correlations and errors and the reduction in the bias support the widespread use of the combined product compared to active or passive products alone (Fang et al., 2016; McNally et al., 2016). Few validation studies have considered active and passive CCI products (Liu et al., 2011; Liu et al., 2012; Fang et al., 2016), whereas a variety of research on the combined product has been published. Pratola et al. (2015) proved that the combined CCI SM product can represent temporal SM variations observed through *in situ* observations in three different dense networks in Ireland, Finland and Spain (REMEDHUS), although these authors used a smaller number of observations. They found good agreements for the Irish network ($R = 0.75$) and REMEDHUS ($R = 0.80$), while poorer results, which were highlighted by negative correlations, were observed over the Finnish site. Dorigo et al. (2015), who also used the same Finnish network, found poor results compared to the combined product, which these authors justified by the strong backscatter variations related to snow freeze-thaw cycles. However, they obtained better correlations in dense networks in Denmark ($R = 0.59$), Korea ($R = 0.63$), China ($R = 0.60$), Australia ($R = 0.66$) and Italy ($R = 0.52$ and 0.63). In these cases, the cRMSDs ranged between 0.03 and 0.08 $m^3 m^{-3}$. All these results agreed with the results in our work, even if the R values were lower.

The merged CCI SM v02.2 product is a combination of active and passive observations that homogenize and merge eight microwave-based products. The individual active CCI SM product includes two active sensors, and the passive CCI SM product includes six passive sensors. Hence, broader bandwidth sensitivity (from 5.25 to 19.3 GHz) and a combination of microwave principles characterize the merged CCI SM product. Moreover, the merged product combines both datasets based on the vegetation density. "Over areas with a low vegetation, the passive dataset is used, while over areas with moderate vegetation density the active is used. In transition areas, where both products correlate well, both products are being used in a synergistic way: on time steps where only one of the products is available, the estimate of the respective product is used, while on days where both passive and active provide an estimate, their observations are averaged" (Dorigo et al., 2015). Thus, the increased temporal sampling density and vegetation discrimination are expected to improve the performance of the combined product compared to individual active/passive products.

3.1.2. Sparse networks

Although REMEDHUS has been considered a dense network, a pixel-scale analysis was also conducted with Inforiego and FluxNet. All the stations that overlapped one pixel were averaged.

The results of this analysis for the active CCI SM v02.2 product over REMEDHUS at pixel scale (Fig. 4) had correlation coefficients between $R = 0.41$ and $R = 0.64$ for the TDR period and between $R = 0.61$ and $R = 0.78$ for the Hydra period, with errors of RMSD~25% and cRMSD~20% during both periods. The results were similar for both Inforiego networks (R between 0.53 and 0.85 and an averaged RMSD and cRMSD of 20%). The bias in this product was close to zero, indicating stable estimations. The correlation results for the FluxNet stations were lower than for the other networks. Only one of the twelve FluxNet stations had a correlation coefficient higher than 0.49. However, the errors were similar. The best land-use results also corresponded to open forest, which could be related to the low-vegetation

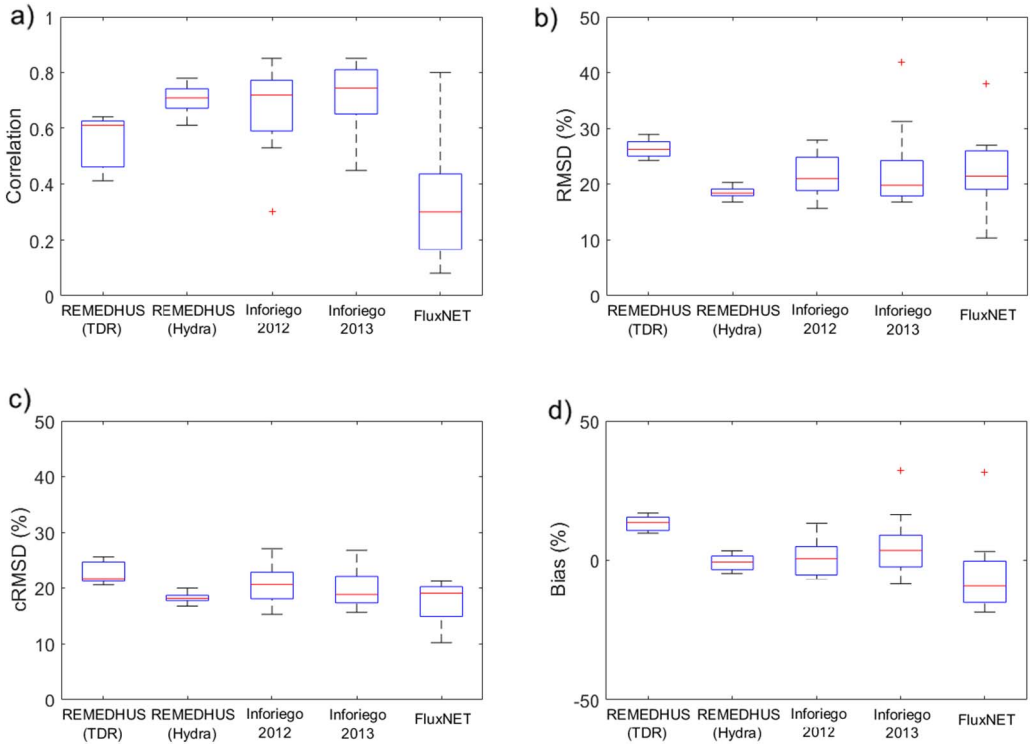

Fig. 4. Box plots of R (a), RMSD (b), cRMSD (c) and bias (d) of the pixel-scale validation for the active CCI SM v02.2 for REMEDHUS, Inforiego and FluxNet.

coverage, but no clear patterns were related to the remaining land uses.

The results of this analysis for the passive CCI product (Fig. 5) revealed an R that ranged between 0.66 and 0.85 for the REMEDHUS TDR data and between 0.70 and 0.79 for the Hydra data. The RMSD were between 0.116 and 0.198 for TDR and between 0.142 and 0.264 for the Hydra data. The cRMSD ranged between 0.087 and 0.107 for the REMEDHUS data from TDR and between 0.078 and 0.108 for the Hydra data. The bias values were between −0.167 and −0.073 for TDR and between −0.241 and −0.109 for the Hydra data, which contrasted the results of the active product (Fig. 4).

The errors for both Inforiego networks (RMSD and cRMSD) were slightly lower than those for REMEDHUS, and the biases had similar

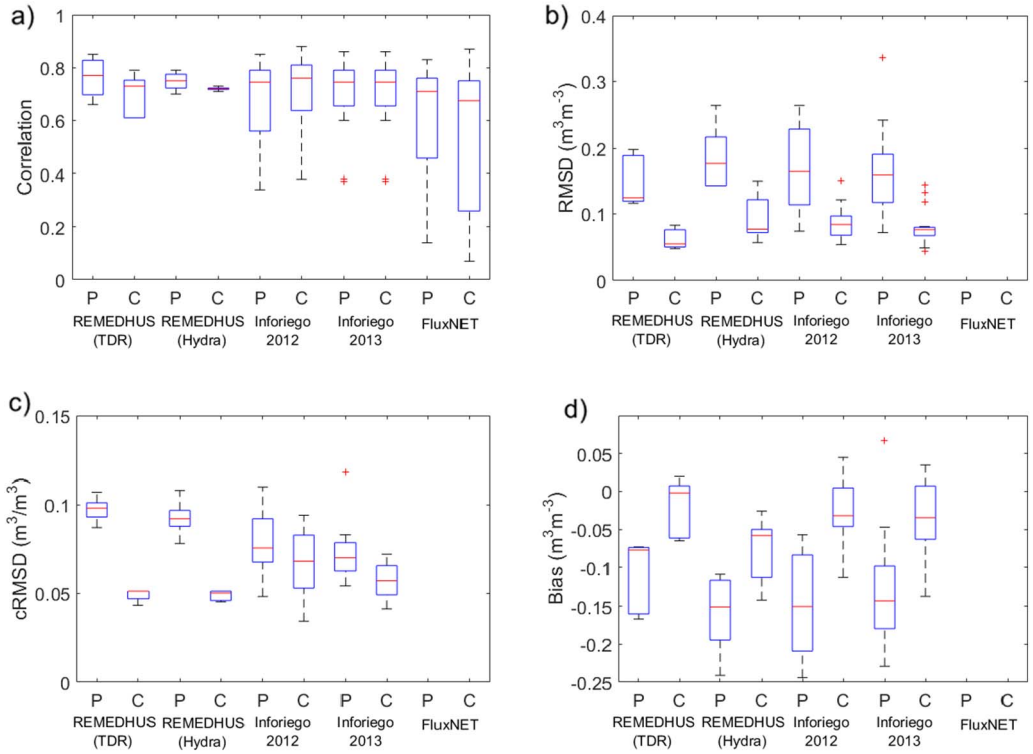

Fig. 5. Box plots of the R (a), RMSD (b), cRMSD (c) and bias (d) of the pixel-scale validation for the passive (P) and combined (C) CCI SM v02.2 for REMEDHUS, Inforiego and FluxNet. Error and bias over FluxNET are not shown due to the different units between stations network and the passive and combined CCI SM products.

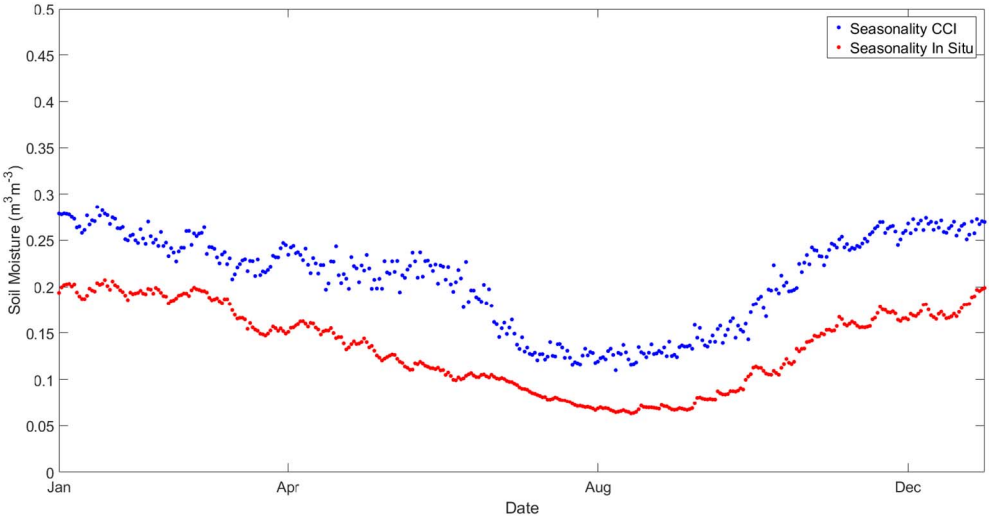

Fig. 6. Seasonality of the combined CCI SM v02.2 time series and *in situ* SM data in REMEDHUS (area-average).

values at all stations, showing the same overestimation trend found in the dense and sparse networks. Wider ranges of R values, errors and biases were observed for the Inforiego12 network compared to Inforiego13 (Fig. 5). In both Inforiego networks, each station corresponded to one CCI pixel, whereas all REMEDHUS was only covered by 5 pixels, which resulted in a low variability for that network. This fact was also observed in FluxNet because the correlation range was wider, varying between 0.14 and 0.83. This variability could have been related to the variety of environmental conditions and land uses in that network. The stations located in open forest (ES-LMa) showed the best correlations (R = 0.83), which were consistent with the better results from the other networks in forested areas (Morille and Rinconada). The stations located in shrub lands also showed better performance (R between 0.54 and 0.71), with results close to those in the forest areas. In contrast, the stations located in pasture (ES-VDA) or agricultural zones (ES-ES2) had the worst correlations (R = 0.14 and 0.24, respectively). The poor results of the ES-ES2 station could be related to the main agricultural land use in this area (rice crop) and the long flooding periods that these soils experience. In addition, the poor results for this station (which is located close to the coast) could also be related to the effect of the land-sea interphase in the SM retrieval, as reported in other studies that used passive sensors (Oliva et al., 2012).

Overall, the passive product exhibited higher variation in the pixel-scale results (Fig. 5) compared to the active product (Fig. 4). However, the mean correlation values were of the same order. The correlation values, but not the errors, are shown for the comparison between FluxNet and the passive CCI SM data because the latter are provided in volumetric units and the FluxNet SM data are measured in percentages.

The validation of the combined CCI SM v02.2 at the REMEDHUS, Inforiego and FluxNet networks (Fig. 5) provided similar correlations as those for the passive product. The correlations varied between 0.61 and 0.79 for REMEDHUS. Similarly, reasonable correlations (R between 0.37 and 0.88) were obtained for the Inforiego networks. Worse results were achieved for FluxNet, which had high variability between sites.

Similar to the comparison for the dense networks, the RMSD, cRMSD and bias were substantially reduced, minimizing the overestimation. However, more outliers were found in the sparse networks, typically for more diverse environmental conditions (*e.g.*, mountainous or semiarid areas for the stations in the Pyrenees and Almeria, respectively). This effect was more remarkable for the combined than for the active and passive products (Figs. 4 and 5). Similar to the passive product, the best correlated land use (R = 0.87) was open forest (ES-LMa station). The low vegetation coverage of this agro-silvopastoral system could be related to the better performance, in a similar to the results for Morille. Again, the worst correlations were obtained at the stations in pasture zones (ES-VDA with an R = 0.27) and some agricultural areas (ES-ES2 with an R = 0.07).

A variety of works, many more than have used active or passive products separately, have validated the combined CCI SM product in different areas of the world using sparse networks. Many of these studies employed networks in China (Peng et al., 2015; An et al., 2016; Su et al., 2016a; Wang et al., 2016) and found correlations between 0.31 and 0.73. Dorigo et al. (2015) used four sparse networks in Africa and found good correlations for the combined CCI SM (R~0.7). In the same study, a correlation of 0.74 was determined in Australia, 0.44 in France, and 0.53 or 0.42 in several networks in the USA. Most had good agreements, but a larger variability in R could be observed than that for dense networks. Nevertheless, these errors remained within the range (0.03 to 0.09) for the sparse networks in our work. These small errors prove the feasibility of the combined CCI SM product under different environmental and climatic conditions.

3.1.3. Analysis of seasonality and anomalies

In this section, the results of the analysis of both seasonality and anomalies of the combined CCI SM v02.2 and *in situ* data over REMEDHUS from 2002 to 2014 (Hydra period) have been carried out.

The *in situ* seasonality is well reproduced by the combined CCI SM (Fig. 6), displaying a decrease in SM values during the dry period and an increase during the wet period, as expected. The *in situ* seasonality is steadier than that of the CCI, which is probably due to the inherent noise of the satellite signals. However, there is a wet bias associated with the combined CCI SM.

The correlation between the seasonality obtained by CCI and *in situ* data is around 0.90 for all the pixels covering the REMEDHUS area, with a correlation of 0.93 for the area-average (Table 4). This result is

Table 4
Correlations between the seasonality and anomalies obtained from *in situ* SM and combined CCI SM v02.2 (pixel-scale and area-averaged) for REMEDHUS (Hydra).

	R	
	Seasonality	Anomaly
Pixel 1	0.92	0.46
Pixel 2	0.93	0.44
Pixel 3	0.87	0.49
Pixel 4	0.92	0.55
Pixel 5	0.94	0.47
Average	0.93	0.57

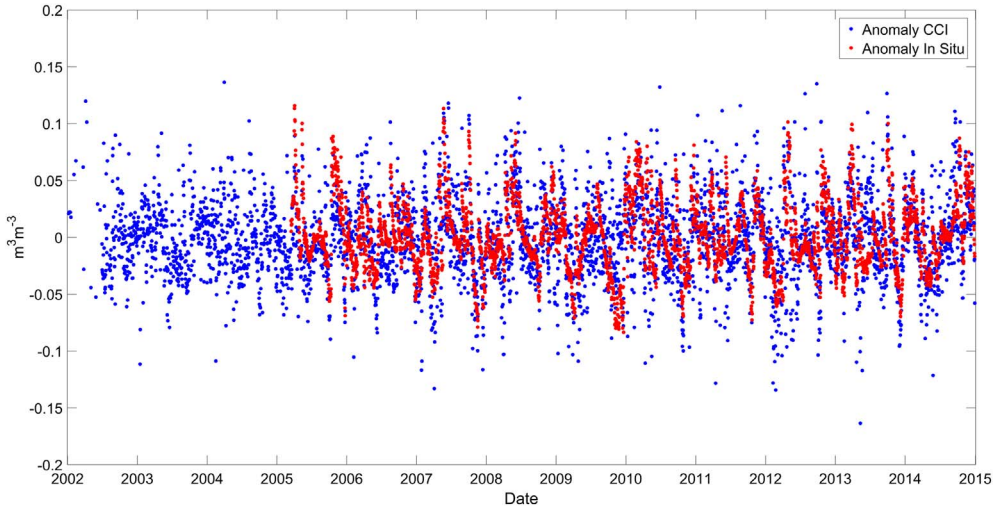

Fig. 7. Anomalies of the combined CCI SM v02.2 time series and *in situ* SM data in REMEDHUS (area-average).

remarkable because in other *in situ* networks worldwide with low soil moisture similar to REMEDHUS, the seasonal comparison with other satellite datasets was of lower quality (Dente et al., 2013).

However, the results of the comparison between anomalies are inconspicuous. The correlation between the combined CCI SM dataset and *in situ* SM is lower than 0.55 for the different pixels that cover the REMEDHUS area, and 0.57 for the area average (Table 4). These results would probably be associated with the larger noise of the satellite signal, as seen in the temporal evolution of both series (Fig. 7). The variability effect produced by the noise is a steady problem in the remote sensing research applied to estimate SM (Su et al., 2015), and it may be caused by RFIs or the small variability range of SM (Dente et al., 2013).

3.2. CCI v02.2 vs. SMOS products (2010–2015)

3.2.1. Comparison over in situ measurements

The passive and combined CCI SM time series (v02.2) were compared with SMOS L2 SM and *in situ* measurements over REMEDHUS (Fig. 8 shows the area average series). All satellite datasets capture well the evolution of the *in situ* SM cycles, although they had a larger dynamic range than the *in situ* time series. While both CCI SM showed overestimation, the SMOS L2 data showed a certain underestimation as regards the *in situ* observations.

For a more detailed analysis, a comparison of the passive and combined CCI and the SMOS L2 SM with regard to the averaged stations within each pixel and DGG (Tables 5 and 6, respectively; only REMEDHUS is shown) was conducted. The correlation coefficients for the both CCI products were similar to those of SMOS L2. However, the error and bias for the combined product were similar to the values that were obtained for the SMOS product, even though those for the passive product were larger. On average, SMOS had a cRMSD value of $0.046\,m^3\,m^{-3}$, whereas CCI had a cRMSD of $0.086\,m^3\,m^{-3}$ for the passive CCI and $0.038\,m^3\,m^{-3}$ for the combined CCI. Although the bias was lower for SMOS, it is interesting to note that whereas the CCI products overestimated the ground measurements (negative bias in Table 5), the SMOS L2 SM underestimated them (positive bias in Table 6), as has been previously observed in the same area (Sánchez et al., 2012; González-Zamora et al., 2015). Similar results were also obtained for Inforiego and FluxNet (not shown).

3.2.2. Inter-comparison of CCI and SMOS products

The results of the inter-comparison between the averages of the SMOS L2 SM product and the passive/combined CCI v02.2 for REMEDHUS showed high correlations (0.74 and 0.79, respectively). However, the increase in bias values between the SMOS and CCI

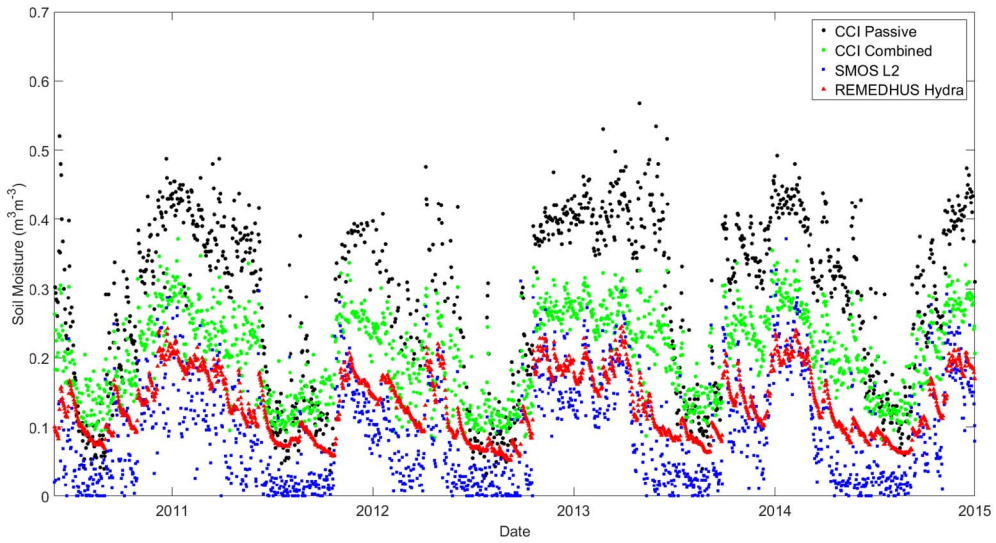

Fig. 8. Soil moisture evolution of the passive and combined CCI SM v02.2, SMOS L2 SM and *in situ* data (area-average) for the REMEDHUS network.

Table 5
Results of the comparison (pixel-scale and area-average) between the *in situ* SM and passive (P) and combined (C) CCI SM v02.2 for the REMEDHUS (Hydra) network. (*) Number of coincident data days. # stations means the number of *in situ* stations within the pixel.

CCI pixel	R		RMSD ($m^3 m^{-3}$)		cRMSD ($m^3 m^{-3}$)		Bias ($m^3 m^{-3}$)		N (days)*		# stations
	P	C	P	C	P	C	P	C	P	C	
Pixel 1	0.85	0.80	0.180	0.077	0.083	0.044	−0.160	−0.063	1058	1454	2
Pixel 2	0.76	0.73	0.203	0.115	0.093	0.045	−0.180	−0.106	1042	1395	11
Pixel 3	0.78	0.75	0.147	0.085	0.074	0.046	−0.127	−0.072	1140	1500	3
Pixel 4	0.77	0.78	0.248	0.127	0.096	0.041	−0.229	−0.120	678	883	1
Pixel 5	0.78	0.77	0.116	0.043	0.087	0.043	−0.077	−0.004	1150	1480	6
Average	0.82	0.81	0.170	0.076	0.086	0.038	−0.147	−0.066	1178	1559	All

Table 6
Results of the comparison (DGG-scale and area-average) between the *in situ* SM and SMOS L2 SM for the REMEDHUS (Hydra) network. (*) Number of coincident data days. # stations means the number of *in situ* stations within the pixel.

SMOS DGG	R	RMSD ($m^3 m^{-3}$)	cRMSD ($m^3 m^{-3}$)	Bias ($m^3 m^{-3}$)	N (Days)*	# stations
1081399	0.65	0.083	0.061	0.055	719	1
1081400	0.76	0.089	0.064	−0.062	714	3
1081401	0.74	0.053	0.050	0.018	682	2
1081912	0.83	0.048	0.048	0.005	697	5
1081913	0.75	0.082	0.048	0.066	696	5
1081914	0.74	0.060	0.046	0.038	656	2
1082425	0.77	0.112	0.053	0.099	700	4
1082426	0.52	0.188	0.102	0.157	319	1
Average	0.82	0.059	0.046	0.037	1607	All

Table 7
Results of the comparison between the combined CCI SM v02.2 and the interpolated maps using *in situ* data for the REMEDHUS (Hydra) network. All the results are significant at the 0.01 confidence level. (*) Number of coincident data days.

CCI pixel	R	RMSD ($m^3 m^{-3}$)	cRMSD ($m^3 m^{-3}$)	Bias ($m^3 m^{-3}$)	N (Days)*
Linear interpolation					
1	0.62	0.077	0.066	−0.040	1439
2	0.77	0.096	0.039	−0.087	1496
3	0.17	0.165	0.073	−0.148	701
4	0.60	0.224	0.159	0.158	1175
5	0.30	0.127	0.103	−0.073	1028
Natural neighbor interpolation					
1	0.67	0.070	0.052	−0.048	1479
2	0.76	0.111	0.041	−0.103	1496
3	0.75	0.094	0.044	−0.083	1492
4	0.66	0.081	0.060	−0.055	1435
5	0.47	0.095	0.079	−0.053	1483
Inverse distance weighting interpolation					
1	0.81	0.086	0.037	−0.078	1480
2	0.78	0.095	0.038	−0.087	1496
3	0.76	0.072	0.041	−0.060	1492
4	0.84	0.065	0.036	−0.054	1435
5	0.77	0.060	0.041	−0.044	1483

products were comparable to those for the comparison with the *in situ* data because of the SMOS underestimation and the CCI overestimation.

The comparison between the CCI pixels and SMOS DGSs over the Inforiego area (2012 and 2013) produced correlations between 0.45 and 0.81 for the passive product (0.77 for the SM series average) and between 0.50 and 0.82 for the combined product (0.83 for the SM series average). These results were similar to those from the REMEDHUS area because both zones have the same land uses (agriculture) and similar environmental conditions. However, when this comparison was conducted over areas with different environmental conditions and land uses, as in FluxNet, the correlations were between 0.25 and 0.58 for the passive product and between 0.19 and 0.81 for the combined product; the highest values were located in the forest areas. In both sparse networks, the biases behaved similarly to those for the dense networks. Clearly, both the combined CCI and SMOS L2 SM products adequately matched, although this comparison analysis should be tested elsewhere with a wider range of land uses and environmental conditions.

3.2.3. Intra-pixel variability

Three interpolated maps of *in situ* SM were daily obtained during the coincident period (2010–2014) at the CCI spatial resolution and other three maps at the SMOS resolution. The objective was to evaluate the effect of the intra-pixel or -DGG spatial variability, following the three interpolation methods. This comparison at the pixel/DGG scale (Tables 7 and 8, respectively) enabled us to study the influence of the spatial distribution within a cell and the performance of the interpolation methods in comparison with the arithmetic mean (Tables 5 and 6).

Generally, different results were found for each interpolation method for both the CCI and SMOS products. The simpler the method, the worse the results became. Thus, one can assume that accounting for the spatial relationships between stations using a complex and geostatistical basis method, such as the weighted distance, may improve the correlations. When the number of stations within a CCI pixel was small (pixels 1, 3, 4 and 5), the average (Table 5) performed better than the simpler methods (linear and nearest neighbor) and identically to IDW (Table 7). However, the three methods perform similarly and slightly better than the average for pixel 2, which encompassed much more stations and thus produced a more detailed spatial pattern.

The influence of the number of stations for the SMOS product was smaller because the difference in the number of stations within a DGG was less pronounced and because the spatial resolution was higher. Thus, the simple average (Table 6) correlated better than the interpolation methods (Table 8), even for the DGGs with denser coverage (DGGs 1081912 and 1081913).

The performance of each interpolation method was sensitive to the number of the stations included in a pixel. Assuming a small number of stations, as in the sparse networks, the simple average could overtake a weak interpolation. The influence of the intra-pixel variability in the results of the validation was clearer in the CCI pixels. In this case, the results recommend considering this variability only if a sufficient number of ground measurements are used to guarantee a robust interpolation. Otherwise, an average value is a reasonable option, as proved through the results in this work.

Several strategies have been used in order to compare satellite observations at coarse spatial resolution with punctual *in situ* measurements. For example, Sánchez et al. (2012) and Kerr et al. (2016) used the direct comparison between point scale measurements against the pixel scale. The average of ground-based observations covered by a pixel was applied by Chan et al. (2016), Al-Yaari et al. (2017), Colliander et al. (2017) and Wigneron et al. (2017). A geostatistical interpolations was used in Colliander et al. (2017). With all these methodologies, the results found were satisfactory. Nevertheless, many other approaches may help to overcome the different spatial resolution of ground and remote measurements. For example, on the use of

Table 8
Results of the comparison between the SMOS L2 SM and the interpolated maps using *in situ* data for the REMEDHUS (Hydra) network. All the results are significant at the 0.01 confidence level. (*) Number of coincident data days.

SMOS DGG	R	RMSD ($m^3 m^{-3}$)	cRMSD ($m^3 m^{-3}$)	Bias ($m^3 m^{-3}$)	N (Days) *
Linear interpolation					
1081399	0.58	0.204	0.107	0.173	1409
1081400	0.56	0.066	0.062	−0.023	1409
1081401	0.68	0.055	0.053	0.016	1312
1081912	0.76	0.112	0.063	0.093	1415
1081913	0.70	0.089	0.053	0.071	1348
1081914	0.71	0.057	0.053	0.022	1169
1082425	0.60	0.127	0.091	0.088	1121
1082426	0.52	0.197	0.143	0.135	1295
Natural neighbor interpolation					
1081399	0.64	0.079	0.064	0.047	1425
1081400	0.68	0.068	0.059	−0.035	1409
1081401	0.71	0.056	0.050	0.027	1319
1081912	0.76	0.118	0.064	0.099	1415
1081913	0.72	0.087	0.052	0.070	1348
1081914	0.74	0.057	0.047	0.032	1234
1082425	0.59	0.147	0.072	0.128	1403
1082426	0.58	0.153	0.086	0.126	1306
Inverse distance weighting interpolation					
1081399	0.81	0.053	0.051	0.016	1426
1081400	0.77	0.052	0.050	0.010	1409
1081401	0.77	0.061	0.046	0.041	1319
1081912	0.78	0.073	0.052	0.051	1415
1081913	0.76	0.069	0.049	0.049	1348
1081914	0.75	0.074	0.045	0.059	1234
1082425	0.77	0.082	0.056	0.061	1403
1082426	0.77	0.076	0.046	0.061	1306

auxiliary imagery to upscale the *in situ* dataset. In this vein, Patel and Srivastava (2015) used synthetic aperture radar (SAR) datasets from Radar Satellite-1 (Radarsat-1) and Environmental Satellite-1 (Envisat-1) Advanced Synthetic Aperture Radar (ASAR) as an interface to upscale the field-level soil moisture at a 25 km × 25 km grid.

3.3. Combined CCI SM v03.2 vs. in situ measurements

The comparison of the combined CCI SM v03.3 with the *in situ* SM time-series from the three dense networks (Fig. 9) revealed that the CCI SM followed well the temporal dynamics and the seasonal patterns of the *in situ* dataset, as previously observed in v02.2 (Fig. 3).

Table 9
Results of the comparison between the *in situ* SM and combined CCI SM v03.2 (area-average) for the Morille, Rinconada and REMEDHUS (TDR and Hydra) networks. All the results are significant at the 0.01 confidence level. (*) Number of coincident data days.

	R	RMSD ($m^3 m^{-3}$)	cRMSD ($m^3 m^{-3}$)	Bias ($m^3 m^{-3}$)	N (days)*
Morille	0.90	0.040	0.038	−0.009	98
Rinconada	0.87	0.041	0.040	−0.005	104
REMEDHUS (TDR)	0.72	0.053	0.045	−0.028	160
REMEDHUS (Hydra)	0.84	0.069	0.035	−0.059	3198

Comparing the results from both versions of the combined CCI product (Tables 3 and 9), it can be seen that the correlation coefficients are similar for all the dense networks. While the bias, RMSD and cRMSD were very similar in Morille and Rinconada, they have been slightly decreased in REMEDHUS, especially the bias (from −0.074 to −0.059), although its sign remains negative, indicating again overestimation. Hence, it can be concluded that the new version of CCI improved the old one. This was expected due to the inclusion of SMOS, since the SMOS SM underestimation may have balanced out the overestimation from the previous version of CCI (Fig. 8), leading to a more accurate estimation in terms of errors and bias.

The validation of the combined CCI SM v03.2 at the sparse networks (Fig. 10) provided higher correlations than those for the previous version. This improvement is remarkable over the FluxNet stations, where the values ranged between 0.48 and 0.92 (an improvement of 30% in some cases) and it is also notable in Inforiego, where some stations obtained a correlation 20% higher than the previous version.

As in the analysis conducted for the dense networks, the RMSD and cRMSD for the v03.2 are slightly lower than for the v02.2 both in REMEDHUS (TDR and Hydra) and Inforiego. However, there was a notable improvement in bias. Although the new version of the combined CCI SM product still showed overestimation over all the networks used, the bias was closer to zero in all networks and periods than the previous version.

Similar to the results obtained for the previous version in FluxNET stations, the best correlated land use was open forest (ES-LMa station, $R = 0.92$); the worst correlations were obtained at the stations in pasture zones (ES-VDA with an $R = 0.48$) and some agricultural areas (ES-

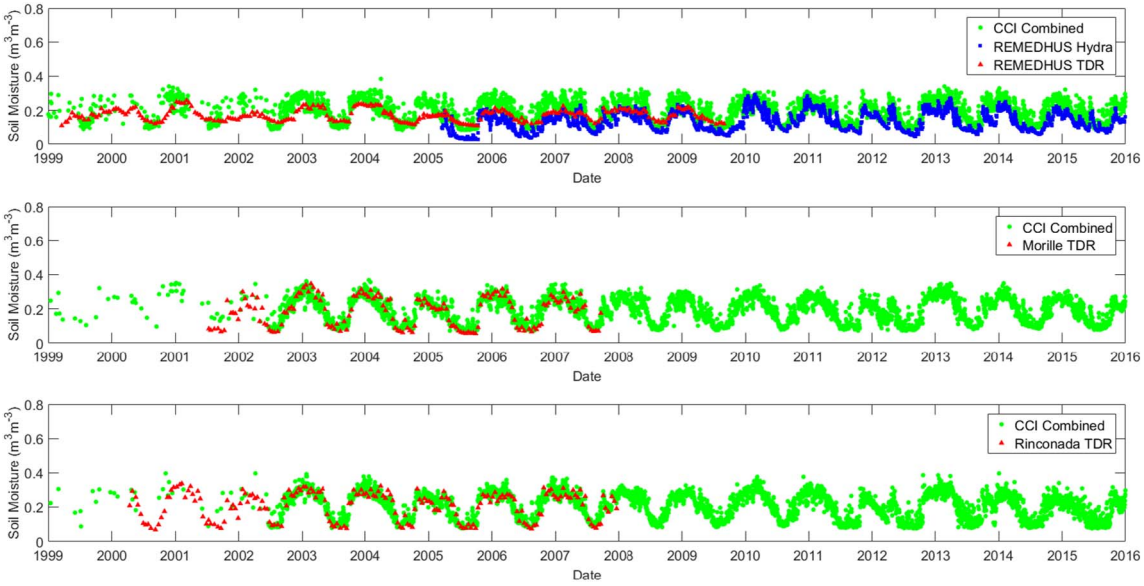

Fig. 9. SM evolution of the combined CCI SM v03.2 and the *in situ* data (area-average) for the REMEDHUS (top), Morille (middle) and Rinconada (bottom) networks.

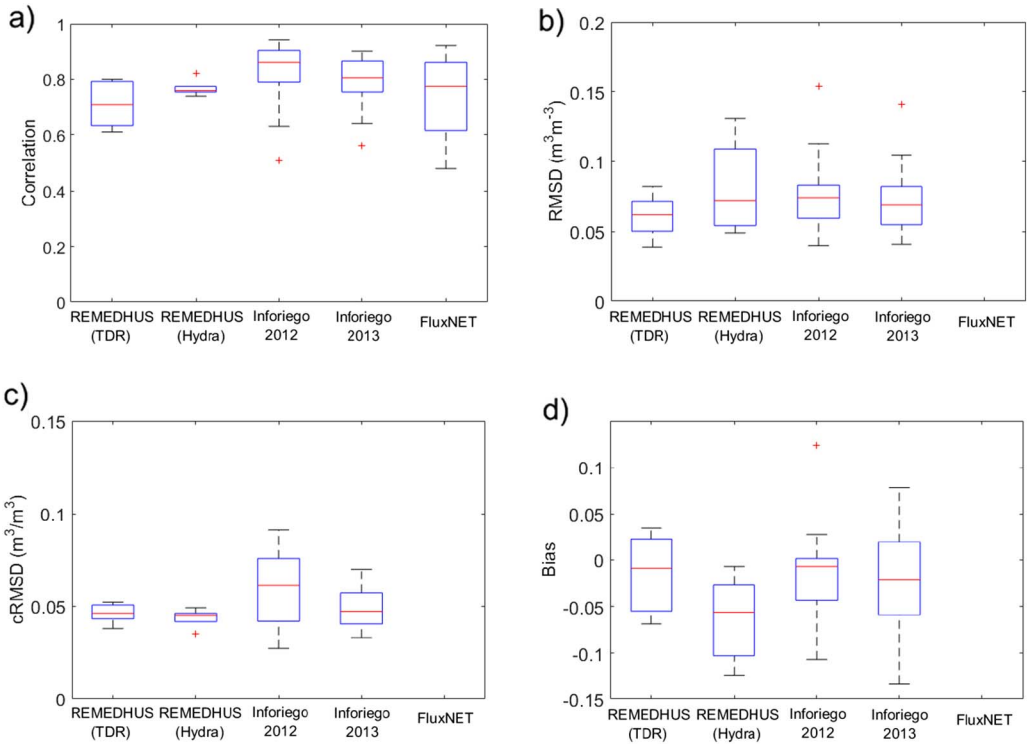

Fig. 10. Box plots of the R (a), RMSD (b), cRMSD (c) and bias (d) of the pixel-scale validation for the combined CCI SM v03.2 for REMEDHUS, Inforiego and FluxNet. Error and bias results over FluxNET are not shown due to the different units between stations network and the combined CCI SM product.

ES2 with an $R = 0.21$). These results continue to be an improvement over the previous version, in which correlations were slightly lower than the new v03.2.

A last remark that should be done regarding the passive and combined CCI products, whatever the version was, is the use of observations acquired by sensors operating at different frequency bands, which, in turn, are related to different soil penetration depths (penetration decreases with frequency). In L-band, it corresponds to the first 5 cm of the topsoil, whereas it is only around the first 1 cm in C-band (Ulaby et al., 2014). Therefore, it is expected that the *in situ* SM measurements at 0–5 cm do not correspond to the soil penetration depth of the X- and Ku-bands (shallower than 1 cm). The ability of microwaves to pass through vegetation canopy is also dependent on frequency, since vegetation attenuates the microwave emission and backscatter from the soil surface (its attenuation increases with frequency). Then, the vegetation may eventually obscure the SM signal at high microwave frequencies (Parinussa et al., 2011). Accordingly, observations below the acceptable quality thresholds are not included in CCI series. In spite of these limitations, the results found in this work show a very good performance, both in term of agreement and errors, of the combined product over a variety of conditions.

4. Conclusions

This research conducted a validation of the three CCI SM v02.2 as well as the combined CCI SM v03.2 products under different spatial and environmental scenarios. Five different *in situ* networks in Spain were used, which included dense and sparse network typologies at small and medium scales. In addition, the CCI SM v02.2 was also compared to the SMOS L2 SM for the coincident period of observations.

The examined CCI v02.2 products adequately captured the temporal series of the *in situ* measurements, showing good agreement in terms of correlations (above 0.85 in the dense networks and ranging between 0.1 and 0.9 for the sparse networks) and errors that were close to the typical accuracy of 0.04 $m^3 m^{-3}$. The poorest results were for the active product, but the agreement in that case should be cautiously evaluated because the SM in this case is a fraction between completely dry conditions (0%) and full saturation (100%) for the topmost centimeters. Therefore, the original ground series had to be converted to normalized units. The passive product, although possessing considerable errors in some cases, exhibited good correlations that were similar to other remote passive missions devoted to SM estimation. Generally, the active and passive CCI series overestimated the ground estimations. Finally, the combined or merged product yielded the best results for both dense and sparse networks. Although good correlations were preserved, the combined CCI greatly reduced the wet biases in the active and passive products separately. Moreover, the seasonality of the ground observations along the whole period were well captured by the CCI series ($R = 0.93$). In addition, the three CCI SM products provided high performance across different land uses and environmental conditions. The stations that were located in most of the agricultural areas and forest areas showed better results, whereas those in pasture locations and certain agricultural conditions obtained the worst results. These comparisons confirmed that the CCI products perform well under a variety of situations, highlighting the usefulness of the combined product over the other two CCI SM products.

The comparative analysis between the CCI v02.2 and SMOS series revealed a very good agreement ($R = 0.83$ on average), although the bias increased with respect to the *in situ* comparison because SMOS underestimated the SM measurements and the CCI product overestimated the measurements. This result afforded some insight about how SMOS could have been improved the new retrieval of the series of CCI, especially regarding the bias balance. Accordingly, the CCI SM v03.2, in which SMOS has been included, represents a notable improvement with respect to the previous version, reducing the bias while maintaining the agreement with the *in situ* datasets. The correlation coefficients obtained are still high for all *in situ* networks used, while the errors remain low. The greatest improvement is observed in the bias, where in some cases it is reduced up to 30%.

The general results of this research may improve knowledge of the

CCI SM data for a wide range of scales and land conditions and its potential applications in many fields.

Acknowledgments

Two projects from the Spanish Ministry of Economy and Competitiveness (Projects ESP2015-67549-C3-3-R and ESP2017-89463-C3-3-R) and one project (SA007U16) from the Castilla y León Region Government and the European Regional Development Fund (ERDF) supported this study. The European Space Agency (Project AO-3230) provided the SMOS data and CCI Soil Moisture products. In particular, we thank Javier Antolín from the ITACyL (Agriculture Technological Institute of Castilla y León) for the Inforiego data services and the FluxNet organization for providing the data from their stations. Finally, the authors thank to the anonymous reviewers for their valuable and useful suggestions that clearly improved the paper.

References

Al-Yaari, A., Wigneron, J.P., Ducharne, A., Kerr, Y., de Rosnay, P., de Jeu, R., Govind, A., Al Bitar, A., Albergel, C., Muñoz-Sabater, J., Richaume, P., Mialon, A., 2014. Global-scale evaluation of two satellite-based passive microwave soil moisture datasets (SMOS and AMSR-E) with respect to land data assimilation system estimates. Remote Sens. Environ. 149, 181–195.

Al-Yaari, A., Wigneron, J.-P., Kerr, Y., Rodriguez-Fernandez, N., O'Neill, P.E., Jackson, T.J., De Lannoy, G.J.M., Al Bitar, A., Mialon, A., Richaume, P., Walker, J.P., Mahmoodi, A., Yueh, S., 2017. Evaluating soil moisture retrievals from ESA's SMOS and NASA's SMAP brightness temperature datasets. Remote Sens. Environ. 193, 257–273.

An, R., Zhang, L., Wang, Z., Quaye-Ballard, J.A., You, J., Shen, X., Gao, W., Huang, L., Zhao, Y., Ke, Z., 2016. Validation of the ESA CCI soil moisture product in China. Int. J. Appl. Earth Obs. Geoinf. 48, 28–36.

Baldocchi, D., Falge, E., Gu, L., Olson, R., Hollinger, D., Running, S., Anthoni, P., Bernhofer, C., Davis, K., Evans, R., Fuentes, J., Goldstein, A., Katul, G., Law, B., Lee, X., Malhi, Y., Meyers, T., Munger, W., Oechel, W., Paw, K.T., Pilegaard, K., Schmid, H.P., Valentini, R., Verma, S., Vesala, T., Wilson, K., Wofsy, S., 2001. FluxNet: a new tool to study the temporal and spatial variability of ecosystem–scale carbon dioxide, water vapor, and energy flux densities. Bull. Am. Meteorol. Soc. 82, 2415–2434.

Bindlish, R., Jackson, T., Cosh, M., Tianjie, Z., O'Neill, P., 2015. Global soil moisture from the aquarius/SAC-D satellite: description and initial assessment. IEEE Geosci. Remote Sens. Lett. 12, 923–927.

Burrough, P.A., 1986. Principles of Geographical Information Systems for Land Resources Assessment. Oxford University Press, New York, pp. 193.

Carrão, H., Russo, S., Sepulcre-Canto, G., Barbosa, P., 2016. An empirical standardized soil moisture index for agricultural drought assessment from remotely sensed data. Int. J. Appl. Earth Obs. Geoinf. 48, 74–84.

Ceballos, A., Scipal, K., Wagner, W., Martínez-Fernández, J., 2005. Validation of ERS scatterometer-derived soil moisture data in the central part of the Duero Basin, Spain. Hydrol. Process. 19, 1549–1566.

Chan, S.K., Bindlish, R., O'Neill, P.E., Njoku, E., Jackson, T., Colliander, A., Chen, F., Burgin, M., Dunbar, S., Piepmeier, J., Yueh, S., Entekhabi, D., Cosh, M.H., Caldwell, T., Walker, J., Wu, X., Berg, A., Rowlandson, T., Pacheco, A., McNairn, H., Thibeault, M., Martínez-Fernández, J., González-Zamora, Á., Seyfried, M., Bosch, D., Starks, P., Goodrich, D., Prueger, J., Palecki, M., Small, E.E., Zreda, M., Calvet, J.C., Crow, W.T., Kerr, Y., 2016. Assessment of the SMAP passive soil moisture product. IEEE Trans. Geosci. Remote Sens. 54, 4994–5007.

Colliander, A., Jackson, T.J., Bindlish, R., Chan, S., Das, N., Kim, S.B., Cosh, M.H., Dunbar, R.S., Dang, L., Pashaian, L., Asanuma, J., Aida, K., Berg, A., Rowlandson, T., Bosch, D., Caldwell, T., Caylor, K., Goodrich, D., al Jassar, H., Lopez-Baeza, E., Martínez-Fernández, J., González-Zamora, Á., Livingston, S., McNairn, H., Pacheco, A., Moghaddam, M., Montzka, C., Notarnicola, C., Niedrist, G., Pellarin, T., Prueger, J., Pulliainen, J., Rautiainen, K., Ramos, J., Seyfried, M., Starks, P., Su, Z., Zeng, Y., van der Velde, R., Thibeault, M., Dorigo, W., Vreugdenhil, M., Walker, J.P., Wu, X., Monerris, A., O'Neill, P.E., Entekhabi, D., Njoku, E.G., Yueh, S., 2017. Validation of SMAP surface soil moisture products with core validation sites. Remote Sens. Environ. 191, 215–231.

Crow, W.T., Berg, A.A., Cosh, M.H., Loew, A., Mohanty, B.P., Panciera, R., de Rosnay, P., Ryu, D., Walker, J.P., 2012. Upscaling sparse ground-based soil moisture observations for the validation of coarse-resolution satellite soil moisture products. Rev. Geophys. 50, RG2002.

Dee, D.P., Uppala, S.M., Simmons, A.J., Berrisford, P., Poli, P., Kobayashi, S., Andrae, U., Balmaseda, M.A., Balsamo, G., Bauer, P., Bechtold, P., Beljaars, A.C.M., van de Berg, L., Bidlot, J., Bormann, N., Delsol, C., Dragani, R., Fuentes, M., Geer, A.J., Haimberger, L., Healy, S.B., Hersbach, H., Hólm, E.V., Isaksen, L., Kållberg, P., Köhler, M., Matricardi, M., McNally, A.P., Monge-Sanz, B.M., Morcrette, J.J., Park, B.K., Peubey, C., de Rosnay, P., Tavolato, C., Thépaut, J.N., Vitart, F., 2011. The ERA-interim reanalysis: configuration and performance of the data assimilation system. Q. J. R. Meteorol. Soc. 137, 553–597.

Dente, L., Vekerdy, Z., de Jeu, R., Su, Z., 2013. Seasonality and autocorrelation of satellite-derived soil moisture products. Int. J. Remote Sens. 34 (9–10), 3231–3247.

Dorigo, W.A., Wagner, W., Hohensinn, R., Hahn, S., Paulik, C., Xaver, A., Gruber, A., Drusch, M., Meckelenburg, S., van Oevelen, P., Robock, A., Jackson, T., 2011. The international soil moisture network: a data hosting facility for global *in situ* soil moisture measurements. Hydrol. Earth Syst. Sci. 15, 1675–1698.

Dorigo, W.A., Gruber, A., De Jeu, R.A.M., Wagner, W., Stacke, T., Loew, A., Albergel, C., Brocca, L., Chung, D., Parinussa, R.M., Kidd, R., 2015. Evaluation of the ESA CCI soil moisture product using ground-based observations. Remote Sens. Environ. 162, 380–395.

Dorigo, W.A., Wagner, W., Albergel, C., Albrecht, F., Balsamo, G., Brocca, L., Chung, D., Ertl, M., Forkel, M., Gruber, A., Haas, E., Hamer, P.D., Hirschi, M., Ikonen, J., de Jeu, R., Kidd, R., Lahoz, W., Liu, Y.Y., Miralles, D., Mistelbauer, T., Nicolai-Shaw, N., Parinussa, R., Pratola, C., Reimer, C., van der Schalie, R., Seneviratne, S., Smolander, T., Lecomte, P., 2017. ESA CCI soil moisture for improved earth system understanding: state-of-the art and future directions. Remote Sens. Environ. 203, 185–215.

Entekhabi, D., Reichle, R.H., Koster, R.D., Crow, W.T., 2009. Performance metrics for soil moisture retrievals and application requirements. J. Hydrometeorol. 11, 832–840.

Entekhabi, D., Njoku, E.G., O'Neill, P.E., Kellogg, K.H., T, C.W., Edelstein, W.N., Entin, J.K., Goodman, S.D., Jackson, T.J., Johnson, J., Kimball, J., Piepmeyer, J.R., Koster, R.D., Martin, N., McDonald, K.C., Moghaddam, M., Moran, S., Reichle, R., Shi, J.C., Spencer, M.W., Thurman, S.W., Tsang, L., Van Zyl, J., 2010. The soil moisture active passive (SMAP) mission. Proc. IEEE *98*, 704–716.

Fang, L., Hain, C.R., Zhan, X., Anderson, M.C., 2016. An inter-comparison of soil moisture data products from satellite remote sensing and a land surface model. Int. J. Appl. Earth Obs. Geoinf. 48, 37–50.

Gao, H., Wood, E.F., Jackson, T.J., Drusch, M., Bindlish, R., 2006. Using TRMM/TMI to retrieve surface soil moisture over the southern United States from 1998 to 2002. J. Hydrometeorol. 7, 23–38.

Gherboudj, I., Magagi, R., Goita, K., Berg, A.A., Toth, B., Walker, A., 2012. Validation of SMOS data over agricultural and boreal forest areas in Canada. IEEE Trans. Geosci. Remote Sens. 50, 1623–1635.

González-Zamora, Á., Sánchez, N., Martínez-Fernández, J., Gumuzzio, Á., Piles, M., Olmedo, E., 2015. Long-term SMOS soil moisture products: a comprehensive evaluation across scales and methods in the Duero Basin (Spain). Phys. Chem. Earth A,B,C 83–84, 123–136.

González-Zamora, Á., Sánchez, N., Martínez-Fernández, J., 2016. Validation of Aquarius soil moisture products over the northwest of Spain: a comparison with SMOS. IEEE J. Sel. Topics Appl. Earth Observ. Remote Sens. 9, 2763–2769.

Gumuzzio, Á., Sánchez, N., Martínez-Fernández, J., 2015. Modeled *vs*. SMOS L2 soil moisture in the central part of the Duero Basin (Spain). In: Lollino, G., Arattano, M., Rinaldi, M., Giustolisi, O., Marechal, J.-C., Grant, E.G. (Eds.), Engineering Geology for Society and Territory - Volume 3: River Basins, Reservoir Sedimentation and Water Resources. Springer International Publishing, Cham, pp. 637–640.

Gumuzzio, Á., Brocca, L., Sánchez, N., González-Zamora, A., Martínez-Fernández, J., 2016. Comparison of SMOS, modelled and *in situ* long-term soil moisture series in the northwest of Spain. Hydrol. Sci. J. 61, 1–6.

Hernández-Santana, V., Martínez-Fernández, J., Morán, C., 2008. Estimation of tree water stress from stem and soil water monitoring with time-domain reflectometry in two small forested basins in Spain. Hydrol. Process. 22, 2493–2501.

Hernández-Santana, V., Martínez-Vilalta, J., Martínez-Fernández, J., Williams, M., 2009. Evaluating the effect of drier and warmer conditions on water use by *Quercus pyrenaica*. For. Ecol. Manag. 258, 1719–1730.

Holmes, T.R.H., De Jeu, R.A.M., Owe, M., Dolman, A.J., 2009. Land surface temperature from Ka band (37 GHz) passive microwave observations. J. Geophys. Res. Atmos. 114 (n/a-n/a).

Jackson, T.J., 1997. Soil moisture estimation using special satellite microwave/imager satellite data over a grassland region. Water Resour. Res. 33, 1475–1484.

Jackson, T.J., Schmugge, T.J., 1991. Vegetation effects on the microwave emission of soils. Remote Sens. Environ. 36, 203–212.

Kerr, Y., Waldteufel, P., Wigneron, J.-P., Delwart, S., Cabot, F., Boutin, J., Escorihuela, M.-J., Font, J., Reul, N., Gruhier, C., Juglea, S., Drinkwater, M., Hahne, A., Martín-Neira, M., Mecklenburg, S., 2010. The SMOS mission: new tool for monitoring key elements of the global water cycle. Proc. IEEE 98, 666–687.

Kerr, Y.H., Waldteufel, P., Richaume, P., Wigneron, J.P., Ferrazzoli, P., Mahmoodi, A., Al Bitar, A., Cabot, F., Gruhier, C., Juglea, S.E., Leroux, D., Mialon, A., Delwart, S., 2012. The SMOS soil moisture retrieval algorithm. IEEE Trans. Geosci. Remote Sens. 50, 1384–1403.

Kerr, Y.H., Al-Yaari, A., Rodríguez-Fernández, N., Parrens, M., Molero, B., Leroux, D., Bircher, S., Mahmoodi, A., Mialon, A., Richaume, P., et al., 2016. Overview of SMOS performance in terms of global soil moisture monitoring after six years in operation. Remote Sens. Environ. 180, 40–63.

Kuria, D.N., Koike, T., Lu, H., Tsutsui, H., Graf, T., 2007. Field-supported verification and improvement of a passive microwave surface emission model for rough, bare, and wet soil surfaces by incorporating shadowing effects. IEEE Trans. Geosci. Remote Sens. 45, 1207–1216.

Lacava, T., Matgen, P., Brocca, L., Bittelli, M., Pergola, N., Moramarco, T., Tramutoli, V., 2012. A first assessment of the SMOS soil moisture product with *in situ* and modeled data in Italy and Luxembourg. IEEE Trans. Geosci. Remote Sens. 50, 1612–1622.

Lagerloef, G., Raul Colomb, F., le Vine, D., Wentz, F., Yueh, S., Ruf, C., Lilly, J., Gunn, J., Chao, Y., deCharon, A., Feldman, G., Swift, C., 2008. The Aquarius/SAC-D mission: designed to meet the salinity remote-sensing challenge. Oceanography 21, 68–81.

Leng, P., Song, X., Duan, S.-B., Li, Z.-L., 2017. Generation of continuous surface soil moisture dataset using combined optical and thermal infrared images. Hydrol. Process. 31, 1398–1407.

Liu, Y.Y., Parinussa, R.M., Dorigo, W.A., De Jeu, R.A.M., Wagner, W., van Dijk, A.I.J.M., McCabe, M.F., Evans, J.P., 2011. Developing an improved soil moisture dataset by blending passive and active microwave satellite-based retrievals. Hydrol. Earth Syst.

Sci. 15, 425–436.
Liu, Y.Y., Dorigo, W.A., Parinussa, R.M., de Jeu, R.A.M., Wagner, W., McCabe, M.F., Evans, J.P., van Dijk, A.I.J.M., 2012. Trend-preserving blending of passive and active microwave soil moisture retrievals. Remote Sens. Environ. 123, 280–297.
Makridakis, S., Wheelwright, S., Hyndman, R., Chang, Y., 1998. Forecasting Methods and Applications, 3rd ed. John Wiley & Sons, Inc, New York.
Martínez-Fernández, J., Ceballos, A., 2003. Temporal stability of soil moisture in a large-field experiment in Spain. Soil Sci. Soc. Am. J. 67, 1647–1656.
McColl, K.A., Vogelzang, J., Konings, A.G., Entekhabi, D., Piles, M., Stoffelen, A., 2014. Extended triple collocation: estimating errors and correlation coefficients with respect to an unknown target. Geophys. Res. Lett. 41, 6229–6236.
McNally, A., Shukla, S., Arsenault, K.R., Wang, S., Peters-Lidard, C.D., Verdin, J.P., 2016. Evaluating ESA CCI soil moisture in East Africa. Int. J. Appl. Earth Obs. Geoinf. 48, 96–109.
Mohanty, B.P., Cosh, M.H., Lakshmi, V., Montzka, C., 2017. Soil moisture remote sensing: state-of-the-science. Vadose Zone J. 16 (1).
Naeimi, V., Scipal, K., Bartalis, Z., Hasenauer, S., Wagner, W., 2009. An improved soil moisture retrieval algorithm for ERS and METOP scatterometer observations. IEEE Trans. Geosci. Remote Sens. 47, 1999–2013.
Njoku, E.G., Jackson, T.J., Lakshmi, V., Chan, T.K., Nghiem, S.V., 2003. Soil moisture retrieval from AMSR-E. IEEE Trans. Geosci. Remote Sens. 41, 215–229.
Ochsner, T.E., Cosh, M.H., Cuenca, R.H., Dorigo, W.A., Draper, C.S., Hagimoto, Y., Kerr, Y.H., Larson, K.M., Njoku, E.G., Small, E.E., Zreda, M., 2013. State of the art in large-scale soil moisture monitoring. Soil Sci. Soc. Am. J. 77, 1888–1919.
Oliva, R., Daganzo, E., Kerr, Y.H., Mecklenburg, S., Nieto, S., Richaume, P., Gruhier, C., 2012. SMOS radio frequency interference scenario: status and actions taken to improve the RFI environment in the 1400-1427-MHz passive band. IEEE Trans. Geosci. Remote Sens. 50, 1427–1439.
Owe, M., de Jeu, R., Holmes, T., 2008. Multisensor historical climatology of satellite-derived global land surface moisture. J. Geophys. Res. Earth Surf. 113 (n/a-n/a).
Parinussa, R.M., Holmes, T.R.H., Yilmaz, M.T., Crow, W.T., 2011. The impact of land surface temperature on soil moisture anomaly detection from passive microwave observations. Hydrol. Earth Syst. Sci. 15, 3135–3151.
Parinussa, R.M., Holmes, T.R.H., Jeu, R.A.M.d., 2012. Soil moisture retrievals from the WindSat spaceborne polarimetric microwave radiometer. IEEE Trans. Geosci. Remote Sens. 50, 2683–2694.
Patel, P., Srivastava, H.S., 2015. An approach to validate soil moisture derived from passive microwave sensors using SAR as an interface. Int. J. Remote Sens. 36 (9), 2353–2374.
Peng, J., Niesel, J., Loew, A., Zhang, S., Wang, J., 2015. Evaluation of satellite and re-analysis soil moisture products over Southwest China using ground-based measurements. Remote Sens. 7, 15729.
Petropoulos, G.P., Ireland, G., Barrett, B., 2015. Surface soil moisture retrievals from remote sensing: current status, products & future trends. Phys. Chem. Earth A,B,C 83, 36–56.
Piles, M., Sanchez, N., Vall-llossera, M., Camps, A., Martínez-Fernández, J., Martínez, J., González-Gambau, V., 2014. A dowscaling approach for SMOS land observations: long-term evaluation of high resolution soil moisture maps over the Iberian peninsula. IEEE J. Sel. Topics Appl. Earth Observ. Remote Sens. 7, 3845–3857.
Piles, M., Petropoulos, G.P., Sánchez, N., González-Zamora, Á., Ireland, G., 2016. Towards improved spatio-temporal resolution soil moisture retrievals from the synergy of SMOS and MSG SEVIRI spaceborne observations. Remote Sens. Environ. 180, 403–417.
Pratola, C., Barrett, B., Gruber, A., Dwyer, E., 2015. Quality assessment of the CCI ECV soil moisture product using ENVISAT ASAR wide swath data over Spain, Ireland and Finland. Remote Sens. 7, 15388.
Rahmani, A., Golian, S., Brocca, L., 2016. Multiyear monitoring of soil moisture over Iran through satellite and reanalysis soil moisture products. Int. J. Appl. Earth Obs. Geoinf. 48, 85–95.
Running, S.W., Baldocchi, D.D., Turner, D.P., Gower, S.T., Bakwin, P.S., Hibbard, K.A., 1999. A global terrestrial monitoring network integrating tower fluxes, flask sampling, ecosystem modeling and EOS satellite data. Remote Sens. Environ. 70, 108–127.
Sakai, T., Iizumi, T., Okada, M., Nishimori, M., Grünwald, T., Prueger, J., Cescatti, A., Korres, W., Schmidt, M., Carrara, A., Loubet, B., Ceschia, E., 2016. Varying applicability of four different satellite-derived soil moisture products to global gridded crop model evaluation. Int. J. Appl. Earth Obs. Geoinf. 48, 51–60.
Sánchez, N., Martinez-Fernandez, J., Scaini, A., Perez-Gutierrez, C., 2012. Validation of the SMOS L2 soil moisture data in the REMEDHUS network (Spain). IEEE Trans. Geosci. Remote Sens. 50, 1602–1611.
Singh, G., Srivastava, H.S., Mesapam, S., Patel, P., 2015. Passive microwave remote sensing of soil moisture: a step-by-step detailed methodology using AMSR-E data over Indian sub-continent. Int. J. Adv. Remote Sens. GIS 4 (01), 1045–1063.
Su, C.-H., Narsey, S.Y., Gruber, A., Xaver, A., Chung, D., Ryu, D., Wagner, W., 2015. Evaluation of post-retrieval de-noising of active and passive microwave satellite soil moisture. Remote Sens. Environ. 163, 127–139.
Su, B., Wang, A., Wang, G., Wang, Y., Jiang, T., 2016a. Spatiotemporal variations of soil moisture in the Tarim River basin, China. Int. J. Appl. Earth Obs. Geoinf. 48, 122–130.
Su, C.-H., Zhang, J., Gruber, A., Parinussa, R., Ryu, D., Crow, W.T., Wagner, W., 2016b. Error decomposition of nine passive and active microwave satellite soil moisture data sets over Australia. Remote Sens. Environ. 182, 128–140.
Ulaby, F.T., Long, D.G., Blackwell, W.J., Elachi, C., Sarabandi, K., 2014. Microwave Radar and Radiometric Remote Sensing. University of Michigan Press.
Vittucci, C., Ferrazzoli, P., Kerr, Y., Richaume, P., Guerriero, L., Rahmoune, R., Vaglio Laurin, G., 2016. SMOS retrieval over forests: exploitation of optical depth and tests of soil moisture estimates. Remote Sens. Environ. 180, 115–127.
Wagner, W., Lemoine, G., Rott, H., 1999. A method for estimating soil moisture from ERS scatterometer and soil data. Remote Sens. Environ. 70, 191–207.
Wagner, W., Hahn, S., Kidd, R., Melzer, T., Bartalis, Z., Hasenauer, S., Figa-Saldaña, J., De Rosnay, P., Jann, A., Schneider, S., Komma, J., Kubu, G., Brugger, K., Aubrecht, C., Züger, J., Gangkofner, U., Kienberger, S., Brocca, L., Wang, Y., Blöschl, G., Eitzinger, J., Steinnocher, K., Zeil, P., Rubel, F., 2013. The ASCAT soil moisture product: a review of its specifications, validation results, and emerging applications. Meteorol. Z. 22, 5–33.
Wang, S., Mo, X., Liu, S., Lin, Z., Hu, S., 2016. Validation and trend analysis of ECV soil moisture data on cropland in North China plain during 1981–2010. Int. J. Appl. Earth Obs. Geoinf. 48, 110–121.
Wigneron, J.-P., Jackson, T.J., O'Neill, P., De Lannoy, G., de Rosnay, P., Walker, J.P., Ferrazzoli, P., Mironov, V., Bircher, S., Grant, J.P., Kurum, M., Schwank, M., Munoz-Sabater, J., Das, N., Royer, A., Al-Yaari, A., Al Bitar, A., Fernandez-Moran, R., Lawrence, H., Mialon, A., Parrens, M., Richaume, P., Delwart, S., Kerr, Y., 2017. Modelling the passive microwave signature from land surfaces: a review of recent results and application to the L-band SMOS & SMAP soil moisture retrieval algorithms. Remote Sens. Environ. 192, 238–262.